Shell-model study of the lattice dynamics of hydroxyapatite

L. Calderín,* D. Dunfield,† and M. J. Stott
Department of Physics, Queen's University, Kingston, Ontario, Canada K7L 3N6
(Received 17 May 2005; revised manuscript received 9 September 2005; published 22 December 2005)

A shell model has been developed and used in a study of the lattice dynamics of hydroxyapatite. The results give insight into the modes of vibration of the lattice, but in addition, the dynamics has been used to obtain quantities involved in x-ray and neutron diffraction patterns and in infrared spectra to help in the interpretation of experimerimental data. Phonons throughout the Brillouin zone were obtained and used to calculate atomic thermal factors entering the x-ray and neutron scattering intensity. The calculated values were in very good agreement with experiment. The phonon modes were also obtained for the Γ-point taking into account the long range Coulomb correction to the dynamical matrix. They were used to calculate the infrared reflectivity for single crystals of hydroxyapatite through the dielectric function and using the dipole approximation, and the powder spectrum was also obtained using the dipole method. Although the positions of peaks in the measured intensities were in good agreement with the frequencies of features in the calculated phonon density of states, the calculated intensities were in poorer agreement with experiment.

DOI: 10.1103/PhysRevB.72.224304 PACS number(s): 63.20.Dj, 78.30.−j, 61.10.Nz, 61.12.Ld

I. INTRODUCTION

Phosphates play an important role in our lives. Not only are there more than two hundred minerals containing phosphate groups finding applications ranging from fertilizers to oral care and in medical industries,[1] but life forms themselves are dependent on them. For example, phosphates play a fundamental role in DNA and energy transfer processes and are a key ingredient of the skeleton.[2] The focus of this study is calcium hydroxyapatite, $Ca_{10}(PO_4)_6(OH)_2$, which is the primary inorganic component of animal bone. The hexagonal structure of hydroxyapatite can be viewed as consisting of unconnected fairly robust PO_4^{3-} tetrahedra with Ca^{2+} in the space between and a column of OH^- ions along the *c* axis to balance the charge. *Ab initio* calculations gave a $P6_3$ space group with all the OH groups aligned, an arrangement which is assumed in this work.[3]

Experimental techniques routinely applied to study the structural properties of phosphates include x-ray and neutron diffraction and infrared spectroscopy, but the interpretation of results involves a knowledge of the dynamical properties of the lattice. The analysis of x-ray and neutron diffraction data involves the thermal factors, and infrared spectra involve a group of the lattice vibrations directly.

The difficulty of obtaining pure single crystal samples of these phosphates means that the materials are often powder samples containing a mixture of phases with low crystallographic symmetry. The analysis of x-ray or neutron diffraction patterns from powder samples is usually performed through a Rietveld refinement in which a large number of parameters are fit to the scattering data. Knowledge of the anisotropic thermal factors for each of the atoms would significantly reduce the number of fitting parameters and improve the reliability of the physical quantities extracted from the experimental data.

The infrared spectrum of a single crystal and its powder differ considerably making the analysis of multiphase powder infrared spectra difficult. A way to assign vibrational modes to observed spectral features in this situation is to use very expensive isotopic substitution in combination with group theoretical analysis.[4] But, the calculation of the phonon frequencies, density of states, their association with particular vibrational modes and ultimately the calculation of the infrared intensities can be a useful alternative to isotopic substitution and could facilitate an accurate interpretation of the infrared data.

The calculation of these diffraction and infrared related quantities requires the phonon frequencies and eigenvectors, and there are two levels at which this can be done: Using either a full quantum mechanical treatment of the electrons in the presence of the ions, or using a classical model for the forces. But, even with today's computers and *ab initio* density functional perturbation theory[5] for the calculation of force constants, dielectric functions and other properties, obtaining reliable results in a reasonable time using these first principles methods is not feasible for systems as large as the ones we are interested in, e.g., apatites and tricalcium phosphates. The alternative is to use parametrized potential models to eliminate the electronic degrees of freedom and consequently the solution of the Schrödinger equation for the electronic structure, which is the most time consuming part in the *ab initio* calculations.

However, *ab initio* methods have been applied to study the ground state crystallographic and electronic structure of calcium phosphates. Hydroxyapatite and related calcium apatites with 40 atoms or so in the unit cell have been investigated,[3] along with the more complex α- and β-tricalcium phosphates with about three hundred atoms per unit cell.[6] But, the dynamical properties of such systems are presently beyond the scope of the *ab initio* methods.

The potential model used in this work is the so-called shell model,[7,8] which consists of replacing each atom or ion in the system by a massive core with a charged massless shell interacting with the core via some potential, usually harmonic. The interaction between cores is Coulombic while each shell interacts with other cores and shells via Coulomb interactions and short-range two- and three-body forces. The

shell model goes beyond a rigid ion model for interatomic forces by including some account of interactions between ions, polarization effects and covalent bonding. The shells are massless so that each follows its core instantaneously and for them the adiabatic approximation holds. With the ojective of studying not just calcium hydroxyapatite but other calcium phosphates we have developed a shell model that can be transferred from hydroxyapatite to these other systems. Section II, which follows, describes the theoretical background of this study and begins with details of the shell model potential that was used.

The calcium phosphates are polar which introduces long range Coulomb splitting of the phonons in the long wave length limit (Γ-point).[9] This requires extension of the dynamical matrix in the shell model to include a long range Coulomb correction. The extension is described in Sec. II, which also gives details of the method for calculating the infrared intensities including the development of an expression for the dielectric function as a function of frequency within the shell model. The calculation of the thermal factors from the phonon frequencies and eigenvectors throughout the Brillouin zone when there are different types of atom in the unit cell is also described.

Section III begins with an evaluation of the available shell models for hydroxyapatite. A new model is then introduced and used to study the lattice dynamics of hydroxyapatite. The results are presented and discussed also in Sec. III, and some concluding remarks complete the paper.

II. THEORETICAL BACKGROUND

A. Shell model potential

Within the shell model the potential energy could include two-, three-, and N-body terms where the bodies that are interacting are understood to be any shell or core in the system. If Z_i and Z_j are the charges of the ith and jth bodies, respectively, and R_{ij} is the distance between them; the two-body part of the interaction potential can be written as:

$$V_{ij} = \frac{Z_i Z_j}{R_{ij}} + A_{ij} \exp\left(\frac{-R_{ij}}{\rho_{ij}}\right) + \frac{C_{ij}}{R_{ij}^n} + \frac{k_{ij}}{2} R_{ij}^2, \tag{1}$$

where A_{ij}, C_{ij}, and k_{ij} are coefficients depending on the nature of the interacting bodies. The first term in Eq. (1) is the Coulomb interaction between the bodies. The second provides a short-range repulsive barrier which prevents ions of different charges collapsing onto each other due to the Coulomb attraction. The third term accounts for van der Waals interactions, and the last provides a harmonic interaction between the ith ion and its massless shell labeled as j. A three body potential describing the effect of directional bonding in the harmonic approximation would be given by:

$$V_{ijk} = \frac{k_{ijk}}{2}(\theta_{ijk} - \theta_0)^2, \tag{2}$$

where the angle θ is measured on the common plane of the three ions, and θ_0 is the equilibrium angle. The total interaction potential, V, is the sum of terms Eqs. (1) and (2) over all the ions and shells in the system.

The coefficients of the potentials are found by fitting experimental and/or theoretical *ab initio* results on, for example, geometry and phonon frequencies, and when there are anharmonic terms, some properties that depend on third-order derivatives such as thermal expansion coefficients. The computer program GULP[10] was used in this study to fit potential parameters, to relax the structure and to calculate off-Γ phonon states. For the calculation of phonon states at the Γ-point the correction[9] due to the long range of the Coulomb potential was introduced into the shell model [Eq. (11)] and required new programming.

B. Phonons

For nonpolar systems and any wave vector $\vec{q}$ the harmonic dynamical problem can be cast into the eigenvalue-eigenvector equation:[9]

$$\omega^2 u_\alpha(n) = \sum_{\alpha' n'} D^{\vec{q}}_{\alpha\alpha'}(nn') u_{\alpha'}(n'), \tag{3}$$

where

$$D^{\vec{q}}_{\alpha\alpha'}(nn') = (m_n m_{n'})^{-1/2} \sum_{ll'} C_{\alpha\alpha'}\begin{pmatrix} nn' \\ ll' \end{pmatrix} \times \exp[-i\vec{q}\cdot(\vec{T}(l') - \vec{T}(l))], \tag{4}$$

is the Fourier transform of the force constant matrix $C_{\alpha\alpha'}\binom{nn'}{ll'}$, which is defined by:

$$C_{\alpha\alpha'}\begin{pmatrix} nn' \\ ll' \end{pmatrix} = \left.\frac{\partial^2 V}{\partial u_\alpha\begin{pmatrix} n \\ l \end{pmatrix} \partial u_{\alpha'}\begin{pmatrix} n' \\ l' \end{pmatrix}}\right|_{\mathrm{o}}. \tag{5}$$

$\vec{T}(l)$ is a crystal translational vector, $\vec{u}\binom{n}{l}$ is the displacement vector of the nth atom in the lth unit cell, and $|_{\mathrm{o}}$ denotes evaluation of the derivative at the equilibrium ion arrangement, and m_n is the mass of the nth atom.

It is straightforward to determine the phonon eigenvalues and vectors throughout the Brillouin zone, but the Γ-point ($\vec{q}=0$) is a special case in polar solids which is addressed later.

C. Thermal factors

The average intensity of a diffracted x-ray beam from a crystal in thermal equilibrium when the scattering vector $\vec{S}$ is a reciprocal lattice vector is given by the following expression:[9]

$$I(\vec{S}) = \sum_{nln'l'} f_n(\vec{S}) f_{n'}(\vec{S}) \exp[i\vec{S}\cdot(\vec{r}(n) - \vec{r}(n'))] \times \exp[i\vec{S}\cdot(\vec{T}(l) - \vec{T}(l'))] \times \left\langle \exp\left[i\vec{S}\cdot\left(\vec{u}\begin{pmatrix} n \\ l \end{pmatrix} - \vec{u}\begin{pmatrix} n' \\ l' \end{pmatrix}\right)\right]\right\rangle, \tag{6}$$

where $f_n(\vec{S})$ is the atomic form factor of the atom n, $\vec{r}(n)$ its position in the unit cell, and $\vec{T}(l)$ is a translational or lattice

vector. The brackets $\langle\ \rangle$ represent an ensemble average. After quantum mechanical ensemble averaging and in the zero-order scattering approximation[9,11] the intensity is written as

$$I(\vec{S}) = \left| \sum_n f_n(\vec{S}) e^{i\vec{S}\cdot\vec{r}(n)} e^{-W_n(\vec{S})} \right|^2, \tag{7}$$

where $W_n(\vec{S})$ is the *Debye-Waller* factor defined as

$$W_n(\vec{S}) = \frac{\hbar}{2Nm_n} \sum_{\vec{q}j} \frac{|\vec{S}\cdot\vec{e}(n|_j^{\vec{q}})|^2}{\omega\left(\begin{matrix}\vec{q}\\ j\end{matrix}\right)} \times \left[\frac{1}{2} + \frac{1}{\exp\left[\hbar\omega\left(\begin{matrix}\vec{q}\\ j\end{matrix}\right) \Big/ k_B T \right] - 1} \right], \tag{8}$$

where N is the number of cells in the crystal, $\vec{q}$ is a vector in the Brillouin Zone, $\vec{e}(n|_j^{\vec{q}})$ is the jth eigenvector of wave vector $\vec{q}$ of the dynamical matrix and $\omega(\begin{smallmatrix}\vec{q}\\ j\end{smallmatrix})$ is the corresponding frequency.

The Debye-Waller factor is usually written as[12]

$$W_n(\vec{S}) = 2\pi^2 \vec{S}\cdot\mathbf{B_n}\cdot\vec{S}. \tag{9}$$

where

$$\mathbf{B_n} = \frac{\hbar}{Nm_n} \sum_{\vec{q}j} \frac{\vec{e}(n|_j^{\vec{q}})\vec{e}(n|_j^{\vec{q}})}{\omega\left(\begin{matrix}\vec{q}\\ j\end{matrix}\right)} \left[\frac{1}{2} + \frac{1}{\exp\left[\hbar\omega\left(\begin{matrix}\vec{q}\\ j\end{matrix}\right) \Big/ k_B T \right] - 1} \right], \tag{10}$$

is the displacement matrix, or the matrix of thermal factors.

The expression for the thermal factors [Eq. (10)] involves a sum over wave vectors in the Brillouin zone. Convergence was achieved summing over 100 points.

D. Γ-point phonons

For polar solids at the Γ-point it is necessary to introduce a correction to the force constant matrix Eq. (5), due to the long-range character of the Coulomb interaction which in the long wave length limit introduces a macroscopic longitudinal electric field in the force constant matrix and, therefore, also in the dynamical matrix.[9]

Although the phonon frequencies at $\vec{q}=0$ may be obtained by straightforward numerical calculation of $\omega(\vec{q})$ at small but finite $\vec{q}$ values by solving Eq. (3) and extrapolating to zero, extrapolation of the eigenvectors to $\vec{q}=0$ if these are also needed, is more complicated. Alternatively, the long wavelength limit of the force constant matrix including the Coulomb corrections may be used to obtain the phonon frequencies and eigenvectors at $\vec{q}=0$ directly.

The force constant matrix in the long wavelength limit taking into account the zero mass of the shells in the shell model[13] and including the Coulomb correction[5,13] is[11]

$$\tilde{C}_{\alpha\beta}(nn') = C_{\alpha\beta}(nn') + \frac{4\pi}{v\epsilon_L^\infty}[\hat{q}f^c(n)]_\alpha[\hat{q}f^c(n')]_\beta + \sum_{n_s'} \left[C^T_{\alpha\beta}(nn_s') + \frac{4\pi}{v\epsilon_L^\infty}[\hat{q}f^c(n)]_\alpha[\hat{q}f^s(n_s')]_\beta \right] \times \sum_{n_s''} [\xi^{s-1}(n_s'n_s'')\xi^c(n_s''n')]_{\alpha\beta}, \tag{11}$$

where α and β denote Cartesian components, n and n_s label the cores and shells, respectively, $C(nn')$ is the force constant matrix between cores n and n' without the macroscopic electric field correction and similarly $C(nn_s)$ and $C(n_sn_s)$ denote core-shell and shell-shell matrices, respectively, $\hat{q}$ is a unit vector in the direction of the wave vector, $f^c(n)$ and $f^s(n_s)$ are the Born charge tensors for the nth core and n_sth shell, respectively, v is the volume of the unit cell, ϵ_L^∞ is the high frequency dielectric constant in the direction of $\hat{q}$ and $\xi^s{}_{\alpha\beta}(n_sn_s')$ and $\xi^c{}_{\alpha\beta}(n_sn)$ are given by

$$\xi^s{}_{\alpha\beta}(n_sn_s') = C_{\alpha\beta}(n_sn_s') + \frac{4\pi}{v\epsilon_L^\infty}[\hat{q}f^s(n_s)]_\alpha[\hat{q}f^s(n_s')]_\beta \tag{12}$$

and

$$\xi^c{}_{\alpha\beta}(n_sn) = C_{\alpha\beta}(n_sn) + \frac{4\pi}{v\epsilon_L^\infty}[\hat{q}f^s(n_s)]_\alpha[\hat{q}f^c(n)]_\beta. \tag{13}$$

The Born charge tensors for the cores and shells are isotropic in the shell model.

Classification of the phonon states is helpful for complicated systems such as hydroxyapatite and there are two main types of method for doing this. The first is based on the site and factor group symmetry analysis, while the second is based on full representations of groups.[14] For Γ-point states in nonpolar solids the symmetry of Γ is used, i.e., the whole point group of the crystal, but for polar solids the classification should be done according to the symmetry of the $\hat{q}$-vector which is in the direction of approach to the Γ-point.[15]

The classification of phonon states based on full group representations is rather abstract and a physical picture is not obvious. However, the availability of the eigenvectors allows the examination of displacement patterns and the projected density of states, which provides information on how groups of atoms or molecules in the system vibrate and what are their characteristic frequencies. This information is useful for the calcium phosphates in which there are robust PO_4 groups whose internal vibrations are a feature of the dynamics. Phonon states are also classified as transversal or longitudinal modes.

E. Infrared spectra

1. Intensities

The infrared intensities were calculated from the Γ-point phonons using two methods. One method used the relation:[16]

TABLE I. Shell models potential parameters for hydroxyapatite.

	Electric charge (e)		
Element	Core	Shell	
P	5.000		
Ca	2.000		
H	1.000		
O	0.860	−2.860	
	Buckingham potential		
Elements	A (eV)	ρ (Å)	C (eV Å^6)
P-O s	845.3	0.3596	
Ca1-O s	1334.0	0.3258	
Ca1-O(H) s	513.9	0.3353	
Ca2-O s	849.3	0.3489	
Ca2-O(H) s	878.8	0.3533	
H-O(H) s	408.7	0.2370	
O s-O s	22894.4	0.1503	32.747
O s-O(H) s	57449.3	0.2094	30.972
O(H) s-O(H) s	92903.2	0.2531	43.612
	Core-shell spring constant		
Element		k (eV/Å^2)	
O		60.82	
O(H)		113.38	
	Three-body potential		
Elements	k (eV/deg^2)	θ_0 (deg)	
O s-P-O s	6.005	109.5	

$$I \approx |\vec{d}|^2, \tag{14}$$

where $\vec{d}$ is the electric dipole moment of the unit cell for a given phonon mode defined as

$$\vec{d} = \sum_n Z_n \vec{e}(n|_j^{\vec{q}}) + \sum_{n_s} Z_{n_s} \vec{e}(n_s|_j^{\vec{q}}), \tag{15}$$

and Z_n (Z_{n_s}) is the electric charge of the nth core (n_sth shell).

TABLE II. Differences between experimental and optimized unit cell parameters of hydroxyapatite.

Parameter	Exp.	Potentials		
		Lee *et al.* (Ref. 19)	Leeuw (Ref. 20)	This work
V (Å^3)	528.0	−6.0	−6.8	0.3
a (Å)	9.4081	0.1354	−0.046	−0.007
b (Å)	9.4081	0.1354	−0.046	−0.007
c (Å)	6.8887	−0.27	−0.02	0.015
α (°)	90.0	0.0	0.0	0.0
β (°)	90.0	0.0	0.0	0.0
γ (°)	120.0	0.0	0.0	0.0
			χ^2	
Unit cell		0.1097	0.0047	0.0003
Atomic positions		0.0190	0.0039	0.0034

The second method was to calculate the reflectivity coefficient from:[17]

$$R = \frac{(1-n)^2 + k^2}{(1+n)^2 + k^2}, \tag{16}$$

where $n = \mathrm{Re}(\epsilon^{1/2})$, $n = \mathrm{Im}(\epsilon^{1/2})$ and ϵ is the dielectric function.

The following expression[11,13] is used for the dielectric function in the shell model including the presence of massless shells, and in the harmonic approximation:

$$\epsilon_{\alpha\beta}(\omega) = \epsilon_{\alpha\beta}^{\infty} + \frac{4\pi}{v} \sum_j \frac{\left[\sum_n G(n)\vec{e}\begin{pmatrix} n \\ j \end{pmatrix}\right]_\alpha \left[\sum_n G^T(n)\vec{e}\begin{pmatrix} n \\ j \end{pmatrix}\right]_\beta}{\lambda_j^2 - \omega^2}, \tag{17}$$

where $\epsilon_{\alpha\beta}^{\infty}$ is the high frequency dielectric function, j labels the Γ-point vibrational modes, and λ_j^2 is the squared frequency of the normal mode j with the Coulomb correction of the force constant matrix set to zero. $G(n)$ is given by the expression:

TABLE III. Thermo-parameters β ($\times 10^{-4}$) of hydroxyapatite at room temperature.

	Experiment (Ref. 22)						Theory					
Atom	β_{11}	β_{22}	β_{33}	β_{12}	β_{13}	β_{23}	β_{11}	β_{22}	β_{33}	β_{12}	β_{13}	β_{23}
P	19	17	25	10	0	0	15	17	22	9	0	0
Ca1	31	31	20	15.5	0	0	26	26	22	13	0	0
Ca2	21	23	30	11	0	0	21	22	47	10	0	0
O1	38	29	52	26	0	0	30	51	44	30	0	0
O2	20	26	73	10	0	0	24	22	90	5	3	2
O3	88	42	50	44	−39	−24	65	53	38	44	−15	−20
O(H)	26	26	99	13	0	0	25	26	57	13	0	0
H	129	129	104	64.5	0	0	83	83	77	41	0	0

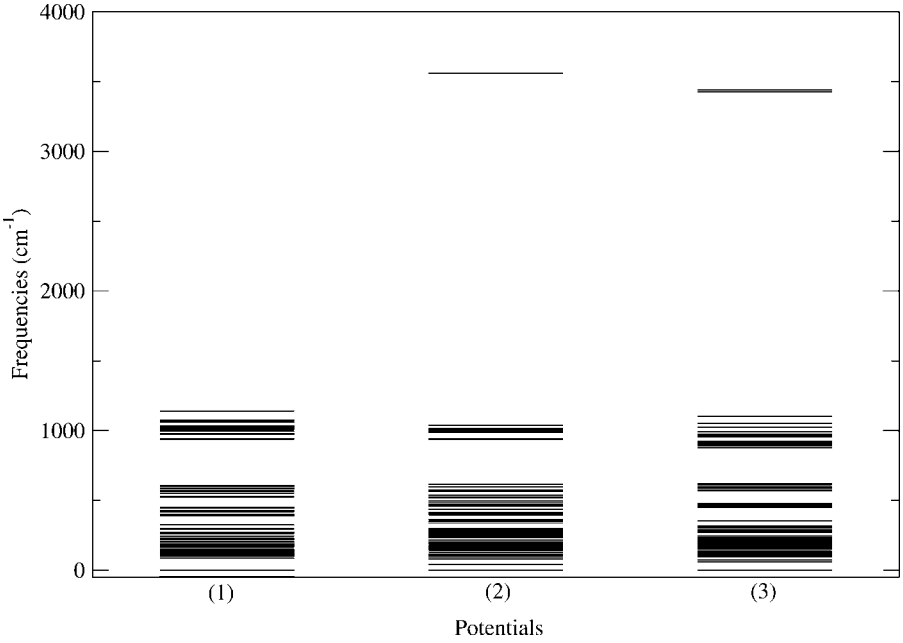

FIG. 1. Comparison of the phonon frequency bands at the Γ-point calculated using the shell models potentials of Lee *et al.* (Ref. 19) (1), Leeuw (Ref. 20) (2) and the new potential reported here (3) for which the potential parameters are given in Table I. The bands below 460 cm^{-1} are due to mixed vibrational modes of PO_4 groups and calcium atoms. The bands between 460 and 1200 cm^{-1} are due to PO_4 vibrations while the narrow band at 3500 cm^{-1} is due to the OH groups.

$$G(n) = \frac{f^c(n)}{m_n^{1/2}} - \frac{1}{m_n^{1/2}} \sum_{n_s n_s'} f^s(n_s) C^{-1}(n_s n_s') C(n_s' n). \quad (18)$$

An *ad hoc* damping term $-i\gamma\omega$ was included in the denominator of expression Eq. (17) to reproduce some effects of anharmonicity on the dielectric function.

2. Assignment of infrared active modes

The infrared active phonon modes are those that transform as the position vector and are, therefore, classified by the corresponding irreducible point representations.[14] It is also customary to use the vibrational modes of isolated molecules to label the infrared active modes. In the case of phosphates the vibrational modes of the isolated PO_4^{3-} molecular ion are used in the classification of some of the infrared active modes.[18]

III. RESULTS AND DISCUSSION

A. Potential parameters

Hydroxyapatite is composed of PO_4 groups linked by calcium ions, and OH ions along the *c* axis. Stoichiometric hydroxyapatite has the space group symmetry of $P6_3^3$. But in refinements of scattering data the $P6_3/m$ group is used together with half occupancies of the OH groups.[1]

Two quite different shell models were developed by Lee *et al.*[19] and Leeuw[20] to study respectively surface relaxation and segregation in hydroxyapatite. Our tests of the first potential[19] gave an imaginary frequency revealing some instabilities. The second potential[19] was also unsatisfactory for our purposes as it used noninteger ionic charges which limited its transferability from hydroxyapatite to other systems of interest. Consequently, a new potential was devised using some potential parameters reported by Meis *et al.*[21] for fluorapatite, and parameters obtained by fitting the observed structure and frequencies of calcium hydroxide. This potential was then refined by a further fitting to the unit cell parameters and atomic positions of hydroxyapatite and the resulting model parameters are listed in Table I. A measure of the error in the fitting was obtained by relaxing the structure. Upon relaxation using the new potential the cell parameters and atom positions changed by 0.007–0.01 Å.

Table II shows the sum of the squared differences between the experimental and theoretical values for the unit cell parameters and the atomic positions for the shell models

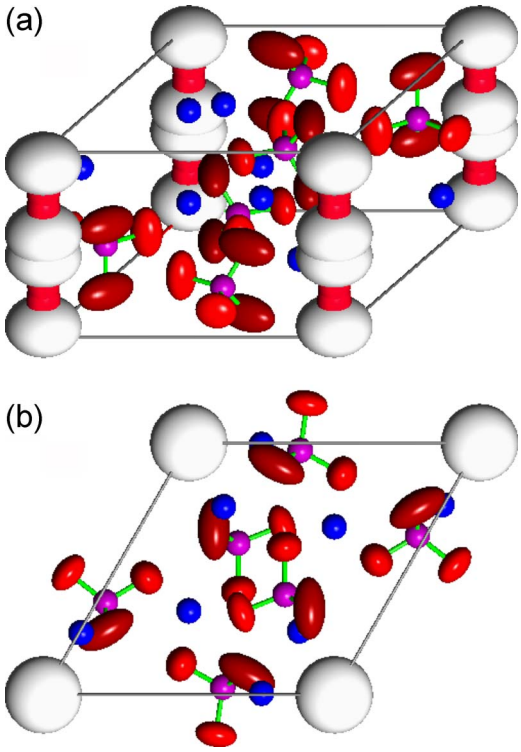

FIG. 2. (Color online) Thermal factors of HA represented by the 99.9% probability ellipsoids. (a) General view; (b) top view.

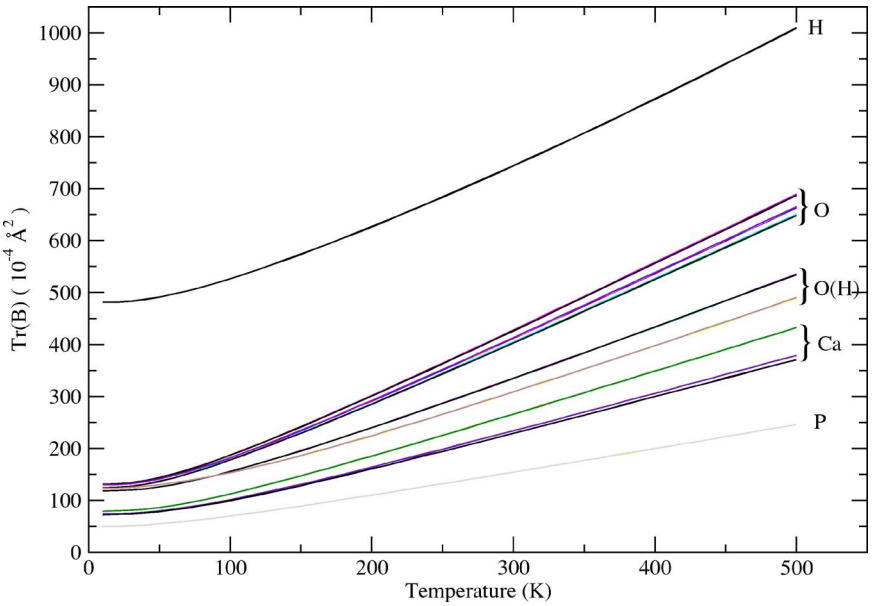

FIG. 3. (Color online) Trace of the thermal factors tensor **B**, Eq. (10), of each atom in the unit cell of hydroxyapatite as a function of temperature.

of Lee *et al.*,[19] Leeuw[20] and the potential used in this work. The first two potentials reproduced the crystallographic structure with an accuracy between 0.04 and 0.3 Å. The calculation of the phonon frequencies at the Γ-point, show that all the potentials lead to stable structures except the first[19] which produced an imaginary frequency as mentioned earlier. But even when the potentials lead to the same structure, there are some significant differences in the phonon frequency bands. For example, as illustrated in Fig. 1, the bands from the new potential contain some features present in the first potential but absent in the second (the distinct PO_4 bands near 500 cm^{-1}), and some features present in the second only (the OH band at 3500 cm^{-1}).

The detailed study of the dynamics of hydroxyapatite that was performed using the new potential (Table I) is reported in the following sections.

B. Thermal factors

The phonon frequencies and eigenvectors off the Γ-point and throughout the Brillouin zone were calculated and used to determine the thermal factors within the harmonic approximation using the results of Sec. II C. The results are given in Table III along with the average of the results obtained from x-ray and neutron diffraction experiments on single crystal samples.[22] The agreement between the experiment and theory is very good but it should be noted that the experimental results were obtained from monocrystals of Holly Springs hydroxyapatite samples which were expected to contain impurities and vacancies.[22] A representation of the thermal factors by the 99.9% probability ellipsoids[23] is shown in Fig. 2. The calcium and phosphorus ions have an isotropic spread while the ellipsoids for oxygen and hydrogen are strongly anisotropic. The O3 and its symmetry

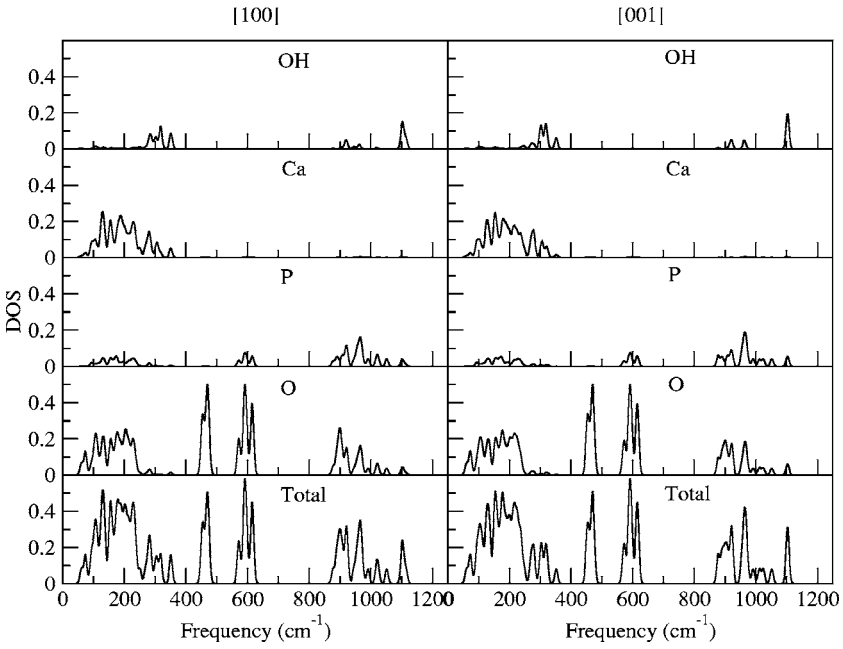

FIG. 4. Projected and total phonon densities of states for the Γ-point approached in the [100] and [001] directions for hydroxyapatite calculated using the shell model (4).

TABLE IV. Classifications of the shell model phonon frequencies (in cm^{-1}) for HA along the [001] direction. The modes are classified according to the irreducible representations of the C_6 point group and also in terms of longitudinal (LO) and transversal (TO) optical modes.

A-modes		B-modes		E_1-modes		E_2-modes	
111.9	LO	60.8	TO	73.4	TO	93.3	TO
127.0	LO	114.9		101.3	TO	106.2	TO
150.4	LO	126.0	TO	125.3	TO	133.1	TO
173.1		157.3	TO	151.8	TO	135.7	TO
189.1	LO	179.6	TO	168.3	TO	154.4	TO
221.0	LO	191.9	TO	176.3	TO	160.4	TO
227.0	LO	199.9	TO	197.4	TO	178.9	TO
247.5	LO	216.1	TO	211.4	TO	186.4	TO
269.2	LO	229.8		215.6	TO	204.2	TO
273.0	LO	236.5	TO	237.0	TO	224.5	TO
322.3	LO	305.6		301.9	TO	279.8	
468.4	LO	352.0		452.0	TO	317.8	
470.3	LO	451.7		471.1	TO	458.2	
575.2	LO	476.2		588.7	TO	468.2	
594.5	LO	588.9	TO	590.0	TO	570.9	
618.4	LO	593.1		613.0	TO	597.5	TO
899.0	LO	615.5	TO	877.4	TO	615.4	TO
967.7		900.1		922.0	TO	890.0	TO
991.1		972.9		955.4	TO	907.9	TO
1011.2	LO	1024.0	LO	962.9	TO	920.2	TO
3442.8	LO	1051.7		1104.2	TO	965.6	TO
		3426.8				1101.7	TO

equivalents (Table III) have a larger ellipsoid than the other oxygens. These are the closest oxygens to the c axis of each PO_4 group and have more room than the rest in which to vibrate. The ellipsoids of the PO_4 oxygens are extended in directions almost perpendicular to the P-O bonds suggesting a rocking motion of the PO_4 group about the phosphorous. The deviation from perpendicular motion is due to the influence of neighboring ions. The light hydrogens have the largest ellipsoids as expected.

One of the objectives of the calculation of the thermal factors from the phonon results was to assist in the Rietveld refinement of powder x-ray and neutron scattering data of low symmetry multiphase powders by reducing the number of parameters required in the fitting. Usually, thermal factors are found from careful diffraction experiments on good single crystal samples. However, in the refinement of powder scattering data the thermal factors are often allowed to vary in the fitting procedure. For systems with low symmetry or which are multiphase there can be a large number of free factors in the refinement which could render the refinement slow or even impossible, and which limits the confidence in the results of even a successful refinement. The input of calculated thermal factors to the refinement could greatly reduce the number of fitted parameters for complicated systems and make a refinement possible. For example, the Reitveld refinement of α-tricalcium phosphate with 312 atoms per unit cell, would be greatly facilitated by the availability of thermal factors. Work is in progress to test this idea for hydroxyapatite and α-tricalcium phosphate.

The thermal factors of hydroxyapatite were also calculated as a function of temperature and the results for the trace of the **B** tensor are presented in Fig. 3. The anisotropy of the thermal factors increases slightly as the temperature is increased. The thermal parameter tensor has $P6_3$ symmetry with three nonequivalent calciums, five nonequivalent oxygens and one nonequivalent hydrogen and phosphorus. The structure has higher symmetry than $P6_3$ for all the atoms except the OH groups and this is reflected in the room temperature thermal factors as well as in the dependency of the thermal factors on temperature, e.g., two of the three nonequivalent calciums in $P6_3$ have very similar thermal properties.

C. Γ-point phonons

The phonon frequencies and eigenvectors were calculated at the Γ-point from the dynamical matrix corrected for the long-range Coulomb field correction as described in Sec. II D. The modes include those that are Raman and infrared active. Because of the correction, the dynamical matrix, and therefore, the phonon states, depend on the direction of approach to the Γ-point, which in the case of infrared absorption, is the direction of propagation of the radiation.

Phonon states were calculated for the Γ-point approached along the principle [100] and the [001] directions of hexagonal hydroxyapatite. The total and projected phonon densities

TABLE V. Classifications of the shell model phonon frequencies (in cm^{-1}) for HA along the [100] direction. The modes are classified according to the irreducible representations of the C_2 point group and also in terms of longitudinal (LO) and transversal (TO) optical modes. Note: A triple transversal degenerate frequency was found around 106 cm^{-1}.

A-modes				*B*-modes			
93.362	TO	317.853		60.8147	TO	350.310	LO
93.383	TO	317.873		73.5139	TO	352.061	LO
111.799	TO	458.207		74.0330		451.763	TO
127.008	TO	458.218	TO	101.392	TO	452.093	
132.270	TO	467.993	TO	114.910	TO	452.102	
133.157	TO	468.245	TO	125.346		471.188	
133.171	TO	468.250	TO	125.391	TO	471.197	
135.779	TO	469.888	TO	126.089	TO	476.279	TO
135.803	TO	570.964	TO	151.890	TO	588.732	
154.403	TO	570.969	TO	152.159		588.804	
154.419		573.177	TO	157.339	TO	588.920	
160.426	TO	594.497	TO	168.356	TO	590.004	
160.432	TO	597.563		172.519	LO	590.008	
173.068	TO	597.568		176.366	TO	593.113	
178.959		615.414		179.668	TO	613.093	
178.984	TO	615.421	TO	190.098		613.099	
186.447	TO	618.490	TO	191.989	TO	615.581	
186.473		890.057	TO	197.490	TO	877.427	TO
188.809	TO	890.080		199.609		899.224	
204.232	TO	898.754	TO	199.960		900.152	
204.251	TO	907.926		211.468	TO	922.107	TO
206.257	TO	907.995		213.951		945.297	
224.586	TO	920.228	TO	215.689	TO	955.431	TO
224.603	TO	920.304	TO	216.197		956.264	
226.516	TO	922.325	TO	229.846	TO	962.965	
228.851	TO	965.673	TO	233.114		972.925	TO
250.462	TO	965.689		236.563	TO	1018.24	LO
269.333	TO	967.896	TO	237.019	TO	1024.02	
279.882		991.132		282.574	LO	1051.73	
279.892		1101.71		301.946	TO	1104.27	
288.055	TO	1101.79		305.662	TO	1114.25	
		3439.34	TO			3426.86	TO

of states which are shown in Fig. 4 are very similar for the two directions, although some differences can be detected. Clearly, the calcium ions only contribute to the low frequency modes (less than 400 cm^{-1}), while the internal motion of the PO_4 and OH groups contribute mainly to states of higher frequency. In particular, the phonon density of states between 450 and 650 cm^{-1} is due almost entirely to the internal motion of the PO_4 groups.

Phonon frequencies and the classification into transverse and longitudinal modes are given in Tables IV and V. The classification according to the irreducible representations of the point symmetry group C_2 of the [100] direction and C_6 of the [001] direction of the wave vector are also given.

For both directions of approach most of the modes are either pure transverse optical (TO) nor pure longitudinal optical (LO). About half of the phonon states for the [001] direction are doubly degenerate due to time-reversal symmetry. These degeneracies are lifted for the [100] direction because of the reduced spatial symmetry, which splits the E_1 (E_2) modes into two B_2 (A) modes. The E_1 modes are split significantly, but E_2 modes very little. While all the B modes of the [001] direction are also present for [100], a large number of A modes for the [001] direction are absent for [100]. Noteworthy was an apparently triple degenerate state along the [100] direction at a frequency of 106 cm^{-1}, with two states coming from the E_2 mode at 106.2 cm^{-1} and a third from the splitting of the 101.3 cm^{-1} E_1 mode.

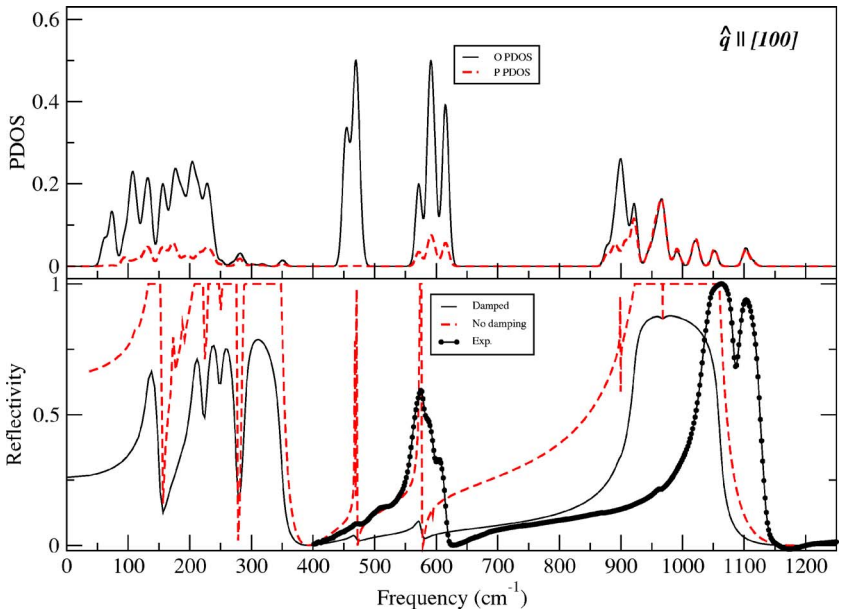

FIG. 5. (Color online) The top panel of this figure shows the [100] projected Γ-point phonon density of states for P and O in hydroxyapatite. The infrared spectra calculated from the dielectric function in the [100] direction with and without damping are shown in the bottom panel. An experimental infrared reflectivity spectrum with the direction of propagation perpendicular to the [001] direction is also shown (Ref. 24).

D. Infrared

1. Monocrystal

The phonons calculated at the Γ-point were used to obtain the infrared reflectivity of a monocrystal of hydroxyapatite for the two main crystallographic directions using the dielectric function approach within the dipole approximation (Sec. II E).

The results are presented in Figs. 5 and 6 for the wave vector along [100] and polarization in the [001] direction, and for the wave vector along [001] and polarization in [100], respectively. Also shown for comparison are the projected phonon densities of states for *P* and *O* for the Γ-point. An experimental infrared reflectivity spectrum for the direction of propagation perpendicular to the [001] direction but otherwise unknown is also given. This is the only measured spectrum for a single crystal of hydroxyapatite that has been found but the polarization is not known and it is unattributed, and should, therefore, be treated with caution.[24]

The correspondence between the features in the projected densities of states shown in the top panel and the experimental spectrum is much closer than for the calculated infrared spectra. In the middle frequency range for which the theoretical spectra are much suppressed the three peaks in the calculated density of states near 600 cm^{-1} due to internal PO_4 vibrations correspond well with the peak in the measured spectrum at 580 cm^{-1} and the two shoulders at slightly higher frequency, given some small frequency shift. The peaks in the density of states at about 460 cm^{-1} could be responsible for the two shoulders at 460 and 500 cm^{-1} in the measured spectrum. In this frequency range features in the density of states do not result in significant intensity in the calculated infrared spectrum. These discrepancies in intensity could be due to the sampling of the different directions

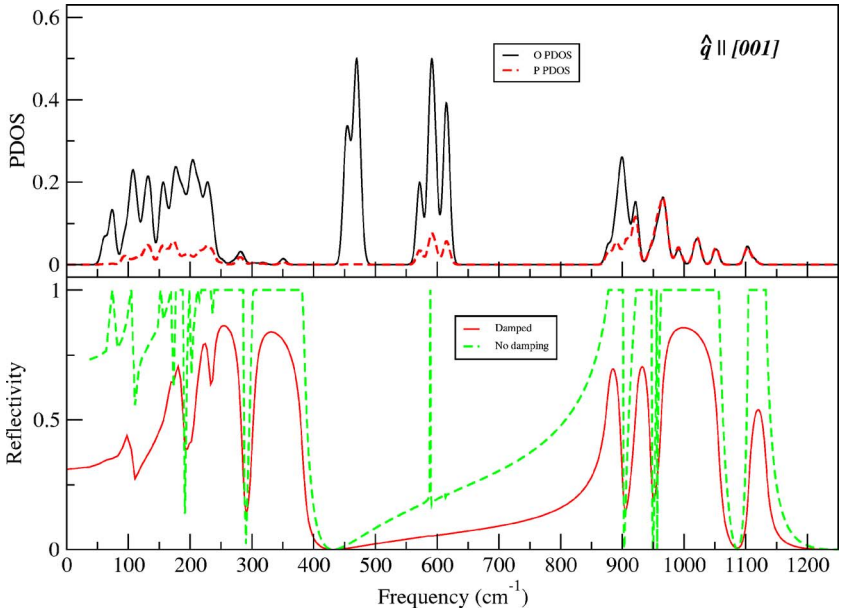

FIG. 6. (Color online) The top panel of this figure shows the [001] projected Γ-point phonon density of states for P and O. The infrared spectra calculated from the dielectric function in the [001] direction with and without damping are shown in the bottom panel.

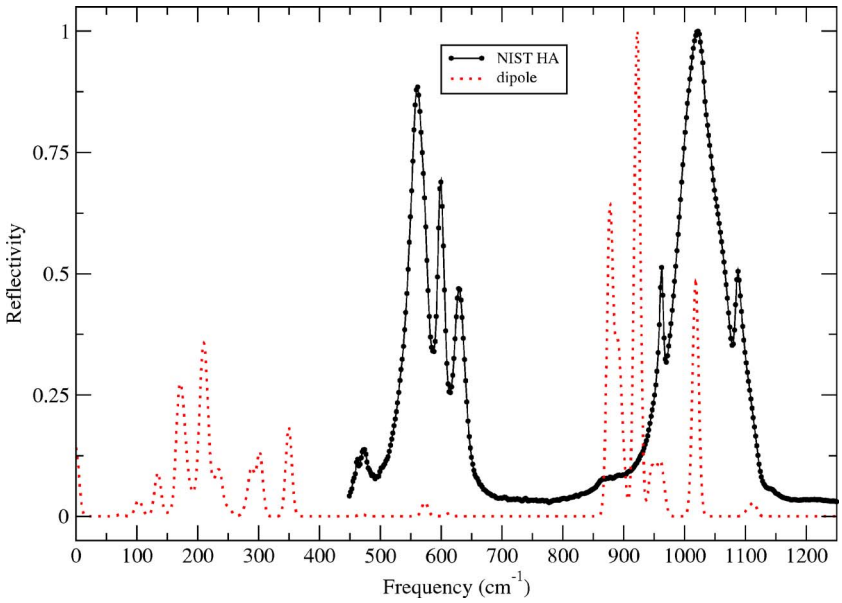

FIG. 7. (Color online) Infrared spectra of a powder sample of hydroxyapatite. The spectrum calculated in the cell dipole approximation, Eq. (14), and an experimental FTIR spectrum of a NIST standard are shown.

of propagation perpendicular to the c axis and/or the absence of polarization of the beam in the experiment, but this is unlikely because, as we shall see shortly, there is a similar discrepancy for the infrared powder spectrum in this middle frequency range. More likely are weaknesses in the step in the theory in which the phonon modes are used to calculate the infrared intensities. For example, multiphonon effects may be poorly represented by the *ad hoc* constant damping term adopted in the calculation of the dielectric function.

The calculated infrared spectrum for the wave vector along [001] shown in Fig. 6 also has two prominent bands, a higher frequency one in the 950–1150 cm^{-1} range and another below 400 cm^{-1}. These result from the phonons contributing to the projected density of states in these frequency ranges. But, very little infrared intensity results from the phonons in the middle frequency range, and it is likely that the intensity in this band is again underestimated. No experimental single crystal data for the [001] direction could be found for a comparison with the calculation performed for that direction.

2. Powder

There are significant differences between powder and single crystal infrared spectra as can be seen from a comparison of the experimental spectra plotted in Figs. 5 and 7. Surprisingly the features in the middle frequency range of the single crystal spectrum are resolved into three sharp lines and a lesser one on the low frequency side, and the two broad peaks in the higher frequency band become a dominant single peak at 1020 cm^{-1} with two symmetrically placed sharp side peaks and weak shoulders at both sides in the powder spectrum. Since a powder consists of randomly oriented crystallites, the sharpness of the lines in the powder spectrum compared with the single crystal is contrary to expectations; the averaging over directions of propagation and polarization should lead to broader features in the powder spectrum. In order to model the infrared powder spectrum the calculated phonons were used within the cell dipole approximation, Eq. (14), to construct the intensity averaged over 81 directions in the Brillouin zone. The calculated and experimental powder spectra are shown in Fig. 7. There is a higher frequency band of sharp peaks and another band below 400 cm^{-1}, but only a very weak feature around 600 cm^{-1}. The observed middle frequency band is again much suppressed in the calculated spectrum.

3. Band assignments

The assignment of the infrared bands for HA have usually been made in terms of the modes of the isolated PO_4 and OH groups, an assignment which comes naturally when the factor group approach is used. PO_4 has a nondegenerate mode labeled ν_1, a double degenerate mode ν_2, and two triply degenerate modes ν_3 and ν_4. In a crystal these degeneracies can be lifted depending on the symmetry of the crystallographic site of the PO_4 group and the direction of propagation of the mode.

In Table VI the factor group based assignment of the infrared bands of hydroxyapatite made by Fowler[4] is shown, along with the assignment of a total reflection Fourier-transform infrared (FTIR) experimental pattern made using Fowler's information, and the assignment based on the analysis of the calculated phonon spectrum. The overall agreement between the experimental and theoretical results is good, although some frequencies are missing from the calculated spectra. But, as mentioned earlier, the infrared spectra of powder and single crystal differ considerably, and the calculation of the intensities from the phonon modes greatly suppresses the middle frequency band.

The availability of phonon eigenvectors as well as frequencies enables a closer connection to be made between observed features in the infrared spectra, phonon modes of the crystal and isolated PO_4 and OH modes. For example, Table VII lists several infrared active modes in the 850–970 cm^{-1} region. Inspection of the atomic displacement patterns shows that four of these are pure PO_4 internal modes and the rest are mixed modes. Five of the mixed ones are

TABLE VI. Assignments of the infrared frequencies (cm^{-1}) of hydroxyapatite in terms of the isolated PO_4 and OH modes.

Experiment[a]	Experiment[b]	Theory
	OH stretching	
3575	3575	3444
	PO_4 ν_3 modes	
1090	1088	1102
1075 sh[c]	1058 sh[c]	not. obs.
1049	1020	1017
1035 sh[c]	1033 sh[c]	not. obs.
	PO_4 ν_1 mode	
964	963	962
	OH librational	
627	630	613
	PO_4 ν_4 modes	
602	598	588
571	561	573,575
	PO_4 ν_2 modes	
475	475	471
463	463	468
	OH stretching	
349	n/a	350
	Ca-PO_4 modes	
323	n/a	322
310	n/a	302
300	n/a	288
283	n/a	282
261	n/a	253
234	n/a	237

[a]Experimental data at −185 °C from Fowler (Ref. 4).
[b]Total reflection FTIR spectrum of hydroxyapatite at room temperature.
[c]sh=shoulder.

PO_4 internal and OH librational combined, while three are a combination of PO_4 and calcium modes. There is one mode that resembles a ν_3 PO_4 mode, but with the oxygen oscillating in anti-phase with the phosphorus fixed. There is also a mode that resembles ν_1 of PO_4 but with the phosphorus also moving.

IV. CONCLUDING REMARKS

A shell model for calcium phosphates has been developed and used to perform a study of the dynamical properties of hydroxyapatite. Phonons throughout the Brillouin zone were calculated and used to determine the thermal factors that enter x-ray and neutron scattering intensity. Good agreement was found with thermal factors obtained from the analysis of single crystal scattering data. This success could prove helpful in the Rietveld refinement of powder scattering data where calculated thermal factors might be used to reduce the number of fitting parameters in the analysis of complex, perhaps multiphase systems, thereby improving the reliability of the fitting.

TABLE VII. Theoretical assignment of phonon infrared active modes contributing to the shoulders in the 850–970 cm^{-1} region.

[001]			
A-modes		E_1-modes	
899.0	ν_4	877.4	OH_L(in phase)+P
967.7	ν_3	922.0	ν_1+OH_L (in phase)
		955.4	ν_3+OH_L (weak)
		962.9	ν_3+OH_L in phase
[100] (*A*-modes)			
890.057	ν_1	922.3	ν_3
890.080	ν_3 (one oxygen fixed)	965.7	ν_3+calciums
898.7	ν_1 (with displacement of P)	967.9	ν_3+calciums
907.9	ν_3+OH_L in phase	991.1	ν_3+calciums
920.2	ν_3+OH_L lib in anti-phase		

An expression for the dynamical matrix at the Γ-point including the long range Coulomb correction was obtained and used to calculate the phonon states at $\vec{q}=0$ approached along the [100] and [001] crystallographic directions. The infrared spectra of a single crystal of HA along the [100] and [001] were calculated from the phonon frequencies and eigenvectors with the dielectric function approach. The calculated infrared spectrum along [100] reproduced some of the features of the experimental data, but calculated intensities in the frequency range 500–600 cm^{-1} due to internal PO_4 motion are greatly suppressed. There is no single crystal experimental data for the [001] direction with which to compare but the intensities in this middle frequency range are much smaller than expected and it is anticipated that the calculated intensities in this range are also poor. The phonon modes and the simpler cell dipole approach,[16] Eq. (14) were used to model the spectrum of HA powder for which a measured spectrum is available, but the agreement between experiment and theory in the middle frequency range was again poor. The poor theoretical IR results in the 500–600 cm^{-1} range could stem from a failure of the fitted shell model to describe some internal motion of the PO_4's, but the positions of peaks in the phonon density of states correspond well with the frequencies of features in the measured spectra and the reason may lie elsewhere. Multiphonon effects are only partially accounted for in the dielectric function approach to the IR spectrum, while they are not included at all in the unit cell electric dipole approach, and the problem may lie here. Incorporation of multiphonon processes may be necessary for an adequate treatment of the damping, frequency shifts and oscillator strengths.

A further point to consider is the use of the harmonic approximation for the motion of the H's. The 99.9% ellipsoids for H shown in Fig. 2 indicate extensive motion at

room temperature of about 1.2 Å in amplitude, and anharmonic effects could be important. At some temperature the motion of the hydrogens in neighboring OH groups might be strongly correlated with each H orbiting its oxygen. The absence of strong directional bonding between a PO_4 and its surrounding Ca ions, might, at higher temperature also lead to rotational motion of a PO_4 group about its central phosphorous. These would be interesting possibilities to explore.

ACKNOWLEDGMENTS

This work is supported by a CRD grant of the NSERC of Canada and Millenium Biologix Corp. L.C. also acknowledges W.A. Miller Materials and Manufacturing Ontario Ph.D. Graduate Award. Fruitful discussions with M. Sayer are also acknowledged.

*Electronic address: calderin@physics.queensu.ca
†Currently at the Brain Research Centre, University of British Columbia, Vancouver, British Columbia, Canada.

[1] J. C. Elliot, *Structure and Chemistry of the Apatites and Other Calcium Orthophosphates* (Elsevier Science, New York, 1994).
[2] P. P. Berlow, D. J. Burton, and J. I. Routh, *Introduction to the Chemistry of Life* (Saunders, Philadelphia, 1982).
[3] L. Calderín, M. J. Stott, and A. Rubio, Phys. Rev. B **67**, 134106 (2003).
[4] B. O. Fowler, Inorg. Chem. **13**, 194 (1974).
[5] S. Baroni, S. de Gironcoli, and A. Dal Corso, Rev. Mod. Phys. **73**, 515 (2001).
[6] X. Yin and M. J. Stott, Phys. Rev. B **68**, 205205 (2003).
[7] B. G. Dick and A. W. Overhauser, Phys. Rev. **112**, 90 (1958).
[8] *Ionic Solids at High Temperatures*, edited by A. M. Stoneham (World Scientific, Singapore, 1989).
[9] A. A. Maradudin, E. W. Montroll, G. H. Weiss, and I. P. Ipatova, *Solid State Physics, Vol. Supplement 3* (Academic, New York, 1971).
[10] J. D. Gale, J. Chem. Soc., Faraday Trans. **93**, 629 (1997).
[11] L. Calderín, Ph.D. thesis, Department of Physics, Queen's University, Kingston, Ontario, Canada, 2005.
[12] K. N. Trueblood, H. B. Bürgui, H. Burzlaff, J. D. Dunitz, C. M. Grammaccioli, H. H. Schulz, U. Shmueli, and S. C. Abrahams, Acta Crystallogr., Sect. A: Found. Crystallogr. **52**, 770 (1996).
[13] J. D. Gale and A. L. Rohl, Mol. Simul. **29**, 291 (2003).
[14] M. J. Lax, *Symmetry Principles in Solid State and Molecular Physics* (Wiley, New York, 1974).
[15] A. A. Maradudin, Phys. Rev. B **13**, 658 (1975).
[16] E. B. Wilson, J. C. Decius, and C. P. Cross, *Molecular Vibrations. The Theory of Infrared and Raman Vibrational Spectra* (McGraw-Hill, New York, 1955).
[17] N. W. Ashcroft and D. N. Mermin, *Solid State Physics* (Saunders, Philadelphia, 1976).
[18] K. C. Blakeslee and R. A. S. Condrade, Acta Crystallogr., Sect. A: Found. Crystallogr. **52**, 770 (1996).
[19] W. T. Lee, M. T. Dove, and E. K. H. Salje, J. Phys.: Condens. Matter **12**, 9829 (2000).
[20] N. H. Leeuw, Phys. Chem. Chem. Phys. **6**, 1860 (2004).
[21] C. Meis, J. D. Gale, L. Boyer, J. Carpena, and D. Gosset, J. Phys. Chem. **104**, 5380 (2000).
[22] K. Sudarsanan and R. A. Young, Acta Crystallogr., Sect. B: Struct. Crystallogr. Cryst. Chem. **25**, 1534 (1969).
[23] M. J. Kronenburg, Acta Crystallogr., Sect. A: Found. Crystallogr. **60**, 250 (2004).
[24] Reflectivitiy apatite spectrum in http://minerals.gps.caltech.edu. Mineral Spectroscopy Server, California Institute of Technology, Pasadena, California, 1999.